ACS Photonics

Article

pubs.acs.org/journal/apchd5

Circular Differential Two-Photon Luminescence from Helically Arranged Plasmonic Nanoparticles

Haobijam Johnson Singh,[†,#] Saumitra,[‡,#] Vijay R. Singh,[‡] Sujit K Sikdar,[§] Balaji Jayaprakash,[∥] and Ambarish Ghosh*[,†,‡,⊥]

[†]Department of Physics, [‡]Centre for Nano Science and Engineering, [§]Molecular Biophysics Unit, [∥]Centre for Neuroscience, and [⊥]Department of Electrical Communications Engineering, Indian Institute of Science, Bangalore 560012, India

ABSTRACT: We report the observation of a circular differential two-photon photoluminescence (TPPL) response from a three-dimensional chiral metamaterial, comprising a system of achiral (spherical) metal nanoparticles arranged on a chiral (helical) dielectric template. The enhanced dipolar response of the individual particles arising from their strong electromagnetic coupling resulted in strong photoluminescence under peak illumination intensities as low as 2×10^3 W/cm^2. The TPPL signal was of approximately equal magnitude but of opposite sign, which depended on both the circular polarization state of the incident beam and the handedness of the helical geometry. The strong chiro-optical effect observed in these experiments may be relevant to technologies related to nonlinear plasmonics, in particular imaging applications where control over the polarization state of the imaged photons may be desirable.

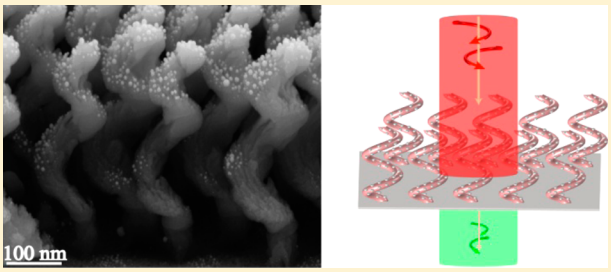

KEYWORDS: *plasmonics, photoluminescence, chirality, two photon, nonlinear, circular dichroism*

Upon illumination with light of appropriate wavelength, metal nanoparticles (NPs) in close proximity can interact strongly with each other via electrostatic coupling of the localized plasmons.[1] Engineering such interactions can provide good control over the properties of electromagnetic waves in both near and far field, resulting in a wide variety of attractive applications pertaining to sensing,[2,3] energy conversion,[4,5] imaging,[6−8] and many more. A particularly well-known example is the presence of a strongly enhanced electromagnetic (EM) field at the junction of closely spaced NPs, which has allowed ultrasensitive detection of various molecular species through surface-enhanced processes such as SERS[9−11] and SEF,[12,13] enhanced photocatalysis,[14,5] and very recently development of photodetectors[15] with unprecedented responsivity, when combined with atomically thin membranes such as graphene. The plasmonic interactions are relevant to collections of NPs as well, where interesting spectral and polarization signatures can be observed and engineered in one-,[16,17] two-,[18] and, very recently, three-dimensional arrays of plasmonic NPs.[19] The geometry of the assembly plays an important role in shaping the optical and crucially the polarization response of the NP assembly. One example particularly relevant to the experiments presented here is the response of a collection of metal NPs arranged in a helical fashion. Under illumination, the EM field at the position of an individual NP has contributions from both the incident and scattered fields from the other NPs, and therefore the overall photoresponse depends on the geometry (chiral symmetry) of both the assembly and the polarization state of the incident beam. This results in a large circular dichroism (CD) where the absorption and scattering of the two circularly polarized states of light by the assembly are different, with equal magnitudes but with opposite signs that depend on the handedness of the helical (chiral) geometry. The magnitude of these effects is significantly larger than most naturally occurring chiral structures, such as proteins and DNA, possibly due to enhanced light−matter interactions typical in plasmonic materials. Such chiral metamaterials are of immense current interest due to their potential applicability in realizing negative index materials,[20] broadband circular polarizers,[21] sensors for chiral biomolecule detection,[22] and many other novel photonic devices.

The response of plasmonic materials to polarized light and their dependence on the system symmetry are not only limited to linear one-photon processes but valid for nonlinear optical processes as well.[23] Of current interest is second-harmonic generation (SHG), or the generation of a photon with twice the energy of the incident, a process that is possible only in noncentrosymmetric systems, and therefore is a powerful tool to probe material symmetries and surface properties. Plasmonically enhanced SHG[24,25] allows such investigations with lower excitation thresholds and could play an important role in the generation and modulation of second-harmonic photons. Apart from SHG, there are other nonlinear processes enhanced by plasmonic NPs, among which two-photon-induced photoluminescence (TPPL) is particularly relevant to this study. In TPPL,[23,26] two photons simultaneously take part in exciting electrons to higher energy levels followed by radiative decay or

Received: February 6, 2016
Published: April 27, 2016

DOI: 10.1021/acsphotonics.6b00087
ACS Photonics 2016, 3, 863−868

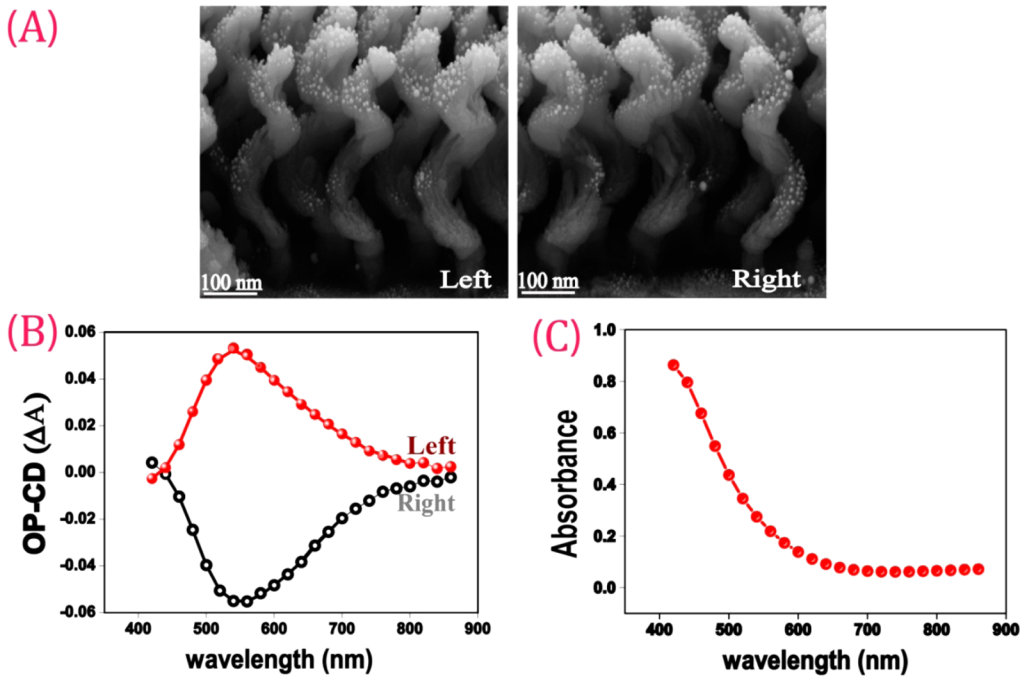

Figure 1. (A) SEM images of silver (seen as white dots) deposited on left- and right-handed helically nanostructured films made of silica. (B) Corresponding measured one-photon circular dichroism (OP-CD) spectra for the left- and right-handed films. (C) Absorption spectra of the left-handed sample showing resonance below 400 nm.

photoluminescence, where photons of different energies are generated. Historically, photoluminescent generation from material systems has been mostly limited to organic dyes and molecules until its discovery in noble metals by Mooradian.[27] Two decades later a systematic study of local field enhancement of photoluminescence in roughened noble metal surfaces was reported by Boyd et al.[28] Since then, a plethora of work has been done on single- as well as two-photon-induced photoluminescence of various noble metal nanoparticle systems such as nanospheres,[29−31] nanorods,[32−36] nanoshells,[37] nanowires,[38,39] and bowtie antennas.[40] A key application of photoluminescent metallic NPs over their organic molecule counterparts is lower photobleaching, which could be beneficial in imaging biological cells.[36,41,42]

While SHG has been observed and studied in detail by various chiroplasmonic systems, for example, in curved gold metal nanowires,[43] twisted cross gold nanodimers,[44] and plasmonic ratchet wheels,[45] in comparison, the origin of TPPL in plasmonic systems of broken chiral symmetry is still unclear. We propose that strong plasmonic interactions between NPs arranged in a helical geometry can give rise to large circular differential TPPL and confirm the same experimentally. Consider circularly polarized photons of energy $\hbar\omega$ incident on a helical assembly of metal NPs. In principle,[46,47] it is possible that the chiral assembly would absorb the circularly polarized light differentially through linear one-photon processes, but in the experimental system described here the one-photon CD at optical frequencies around $\hbar\omega$(800 nm) was found to be negligible. On the other hand, the luminescent photons with energies slightly lower than $2\hbar\omega$ could be strongly enhanced via plasmonic interactions, which caused the TPPL to depend on the symmetry of the NP assembly. This gave rise to circular differential TPPL, which was approximately equal to and of opposite sign of the two enantiomers of the helical arrangement. In this context, it must be mentioned that circular differential photoluminescence has previously been observed in chiral (helical) inorganic nanostructured films,[48] a system without any plasmonic component.

RESULTS AND DISCUSSIONS

The experimental system consisted of silver (Ag) NPs decorated on a helical template made of a dielectric material (SiO_2). The SEM images for the two enantiomers of the helical film are shown in Figure 1A, where the white dots correspond to the silver nanoislands. The method of fabrication has been reported before,[47] and the procedures adopted to prepare the samples reported here are discussed in the Methods section. In short, we used glancing angle deposition (GLAD)[49] to fabricate left- and right-handed helically nanostructured thin films on a glass substrate. Subsequently, the substrate was rotated to deposit small islands of silver on the silica helices, resulting in a helical arrangement of silver nanoislands where the geometry of the helix could be controlled. A key advantage of this technique is the possibility of having a (one-photon) chiro-optical response in the visible regime, due to the small size of the metal NPs, as opposed to chiral nanostructures made of metallic materials. Also, this technique allowed high flexibility in tuning the spectral positions of the chiro-optical response, through simple annealing[50] or varying the underlying dielectric[51] material of the helix. In Figure 1B, we show the measured circular dichroism, defined as the difference in absorption for normally incident left (A_L) and right (A_R) circularly polarized (CP) light, given by CD[46,43] = $A_L - A_R \approx 2(I_L - I_R)/(I_L + I_R)$. The approximate form of CD can be obtained for small differences between A_L and A_R, which can be represented as the ratio of two measurable quantities, given by the difference between intensities of the transmitted light for the two CP components ($I_L - I_R$) to the average transmitted intensity (= $(I_L + I_R)/2$). While the CD response of just the dielectric silica helices was very weak and cannot be measured

DOI: 10.1021/acsphotonics.6b00087
ACS Photonics 2016, 3, 863−868

with our measurement setup, the CD spectra of the silver-decorated helices show a bisignated[52] response around the absorbance peak (400 nm, Figure 1C). Due to limitations in our experimental measurement setup, the CD band below 400 nm cannot be measured and the band at 550 nm as seen from Figure 1B shows almost equal and opposite sign for the two-handed samples. For wavelengths greater than 840 nm the CD response reduces to indeterminable values.

A schematic of the experimental design to investigate the nonlinear chiro-optical properties of the helically nanostructured films is shown in Figure 2A, and the optical path

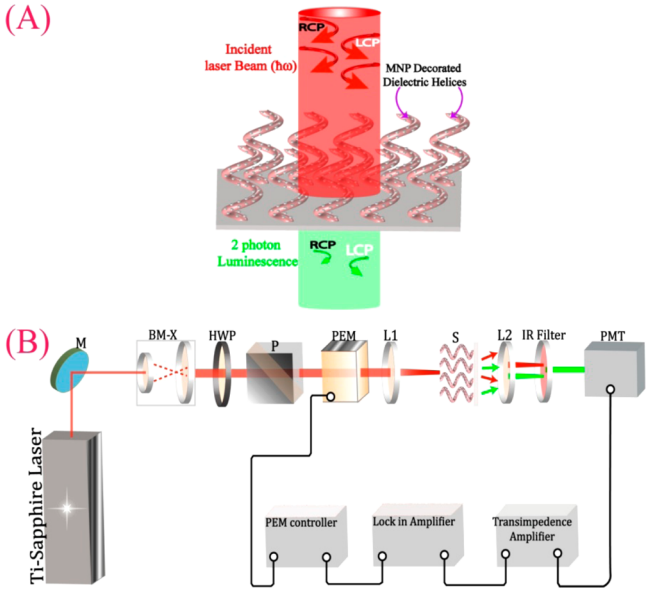

Figure 2. (A) Schematic of the experiment: An intense beam of photons of energy $\hbar\omega$ (shown in red) modulated between the two circular polarized states was incident normally on the sample consisting of dielectric helices coated with metal NPs. A short-pass filter allowed energies higher than $\hbar\omega$ (shown in green) to go through, which was detected by a photodetector or analyzed by a spectrometer. (B) Schematic of the experimental setup for measuring two-photon photoluminescence circular dichroism (TPPL-CD): M (mirror at 45°), BM-X (beam expander), HWP (half-wave plate), P (polarizer), PEM (photoelastic modulator), L1-L2 (focusing lens), S (sample), IR filter (copper sulfate solution), PMT (photomultiplier tube).

through various components of the experimental setup is shown in Figure 2B. Further details are given in the Methods section. Typically the wavelength of the fundamental beam (shown in red) incident normally on the sample varied between 800 and 1000 nm, and the average power was between 25 and 100 mW focused to a spot size of 5×10^{-4} mm^2 on the sample. The polarization of the incident beam was modulated between the two circularly polarized states at 50 kHz. A short-pass filter (consisting of saturated copper sulfate solution) only allowed wavelengths shorter than 600 nm to pass through (shown in green), which was either detected by a PMT or analyzed spectrally (not shown in Figure 2B). The main aim of the experiment was to measure the difference in the two-photon photoluminescence for the circularly polarized states of the incident beam. This difference was quantified through TPPL-CD[53,54] (two-photon-induced photoluminescence circular dichroism), which is defined as the ratio of two measurable quantities, the difference of photoluminescent intensity for two circularly polarized states with an incident beam, $I_L^{TPIPL} - I_R^{TPIPL}$ to the average transmitted photoluminescence intensity $(= (I_L^{TPPL} + I_R^{TPPL})/2)$, such that TPPL-CD $= 2(I_L^{TPPL} - I_R^{TPPL})/(I_L^{TPPL} + I_R^{TPPL})$.

Before measuring the TPPL-CD, it was necessary to check if there were photons generated due to nonlinear processes and to characterize it further. For an incident beam of wavelength 800 nm, we imaged the sample through the short-pass filter (inset of Figure 3A) and could clearly see a green color, implying a nonlinear luminescence signal. For further characterization, we analyzed the PL spectrum, and the results are shown in Figure 3A. The nonlinear PL spectrum showed a small difference for two excitation wavelengths of 800 and 1000 nm. More importantly, we could not see any signature of second-harmonic generation, which would have appeared at 400 and 500 nm for the two incident photon energies, respectively. It is likely that the low strength of the SHG signal was partially due to the small size of the silver NPs. The comparatively larger PL signal was possibly due to plasmonic enhancement[28,35,55] of the particle dipole moments from their electromagnetic coupling, where the radiative decay rate for transitions around 500 nm was enhanced due to this enhanced dipolar response of the individual particles.

The PL signal measured on the PMT showed a slow decay, especially for higher laser powers, signifying bleaching processes. To characterize this further, we measured the PL response as a function of time for different powers of the linearly polarized incident beam (wavelength 800 nm). The bleaching was significant for laser powers greater than 100 mW, where the signal decreased by almost a factor of 2 over a duration of 10 s. Accordingly, in all the measurements of TPIPL-CD we kept the incident powers less than 100 mW. The inset of Figure 3B shows the log–log plot of the measured PL signal as a function of incident laser power at three different instants of data acquisition (marked as a, b, c). A slope of 2 verifies that the measured PL signal was indeed a two-photon-induced phenomenon.

In Figure 4, we show the measured TPPL-CD for a range of wavelengths between 800 and 900 nm for left- and right-handed samples. The incident laser power was fixed at 25 mW to ensure low bleaching. The TPPL-CD was of similar magnitude but opposite signs for the two samples, as would be expected in a chiro-optical effect. The strength of the CD signal remained independent of the power of the incident beam (not shown). The samples showed a spot-to-spot variation of about 35% in the TPPL-CD, as measured over six different spots at a fixed wavelength of 800 nm and power 100 of mW. This is slightly larger than the variation in one-photon CD, which typically had a spot-to-spot variation of 15% and is probably due to added variability arising due to bleaching effects. To elaborate on the physical mechanism of the observed TPPL-CD response, it is possible that the luminescence signals from individual NPs were enhanced due to plasmonic, here dipole–dipole, interactions from NPs in close proximity. The dipolar interactions are expected to be sensitive to the geometrical arrangement of the NPs as reported in recent one-photon studies[46,47,56] of helically arranged NPs under circularly polarized illumination, as well as the phases of the individual dipoles, resulting in a dependence of the TPPL signal on the circular polarization state of the incident beam. Note the magnitude of the TPPL-CD obtained in our experiments is expected to depend strongly on the incoherent contributions to the decay processes. To compare the strength of the effect with that of existing systems, the highest TPPL-CD

DOI: 10.1021/acsphotonics.6b00087
ACS Photonics 2016, 3, 863–868

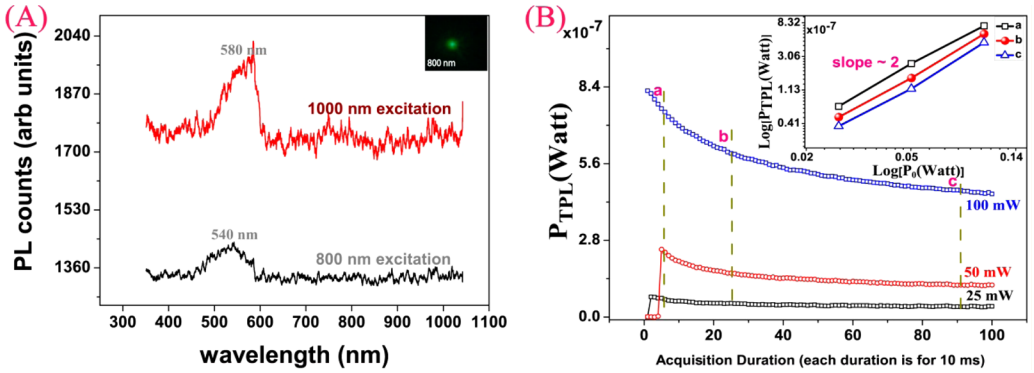

Figure 3. (A) Photoluminescence (PL) spectra of a sample acquired by a fiber-based (Ocean Optics) spectrometer at two different excitation wavelengths. The spectra were acquired at a laser power of 150 mW. Inset shows the image of the PL signal captured by a CCD camera at 800 nm excitation wavelength. (B) Measured power (P_{TPL}) of the two-photon PL signal for three different laser powers at 800 nm excitation to investigate the extent of bleaching at high laser power. Inset shows a log−log plot of the measured PL signal as a function of incident laser power at three different instants of data acquisition (marked as a, b, c). A slope value of 2 verifies that the measured PL signal was indeed due to a two-photon process.

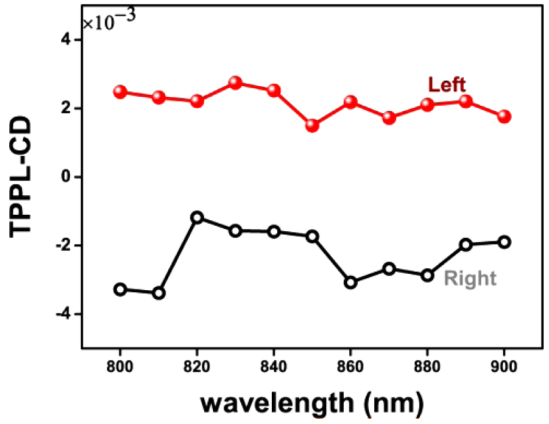

Figure 4. Measured TPPL-CD spectra as a function of incident laser wavelength for the left and right samples at a fixed incident power of 25 mW.

values are obtained with systems containing chiral supramolecules. Examples include enantiopure chiral polyfluorene thin films where a TPPL-CD value (anisotropy) as high as 0.034 was observed around 405 nm.[57] Similarly large two-photon circular dichroism has also been reported in azo compounds,[58] hexahelicene derivatives,[59] (*R*)- and (*S*)-bi(2-naphthol),[60] etc. In addition to these chiral supramolecular systems, a TPPL-CD response of around 0.04 was also reported for Gd^{3+} in a single uniaxial crystal of $Na_3[Gd(C_4H_4O_5)_3]\cdot 2NaClO_4\cdot 6H_2O$.[61] In contrast to all the systems mentioned above, the luminescent sources reported here (silver NPs) are essentially achiral, and the large circular differential signal arises purely due to plasmonic interactions between the resonantly enhanced plasmonic dipoles.

CONCLUSIONS

In summary, we have demonstrated the two-photon-induced chiro-optical photoluminescent response from a three-dimensional chiral metamaterial consisting of achiral silver nanoparticles decorated on a dielectric chiral (helical) template made up of SiO_2. The measured TPPL-CD shows opposite and approximately equal behavior for left- and right-handed films, and as far as we know, this is the first demonstration of TPPL-CD in a plasmonic system. The experimental system presented here has been considered for biomedical applications in recent times, where similar helical[62] nanostructures have been rendered magnetic[63,64] and thereafter propelled noninvasively in biofluids.[65] Accordingly it is natural to wonder whether the large TPPL observed here can be useful in imaging these nanostructures (often referred to as nanoswimmers in the literature) under in vivo conditions. The observed TPPL-CD provides an interesting possibility in imaging applications, where the signal intensity can depend on polarization of the incident fundamental beam and perhaps on the presence of chiral molecular species in close vicinity.

METHODS

Sample Fabrication. We used a physical vapor deposition based technique known as glancing angle deposition[49] to fabricate the samples. First a dielectric helical template made up of SiO_2 (∼300 nm height) was fabricated using a conventional GLAD setup where the incoming vapor source (0.1−0.2 nm/s) was allowed to be incident at an extreme angle of 84° to a rotating (0.05−0.1 rpm) glass substrate. This process is then followed by a small amount (∼5 nm) of metal (Ag) deposition (∼0.01 nm/s) on the same glass substrate, which is now kept at an angle of 5° with respect to the vapor source. This results in the formation of small isolated metal islands on the surface of the dielectric helices due to a self-shadowing effect. The pressure of the chamber was kept below 5×10^{-6} mbar during the evaporation.

Optical Characterization. The optical characterization of the metal-decorated helices was performed by measuring both their linear (circular dichroism) as well as nonlinear (two-photon-induced photoluminescence-CD) chiro-optical activity.

One-Photon Circular Dichroism. The one-photon CD measurement of the samples was performed in a system comprising a lamp and a monochromator (Horiba Yvon), photoelastic modulator (Hinds Instruments), and a Si photodiode (Thorlabs). Light of a particular wavelength emitted from the monochromator was sent through the photoelastic modulator, resulting in a modulation between left and right circularly polarized states at 50 kHz. This beam (diameter ∼5 mm^2) was transmitted normally through the substrate and then focused on to the photodetector. The cable lengths and the load resistance across the photodiode were kept sufficiently low to ensure the temporal response of the detector to be faster

DOI: 10.1021/acsphotonics.6b00087
ACS Photonics 2016, 3, 863−868

than 150 kHz. The CD signal was measured using a lock-in amplifier (Signal Recovery 7270) through standard phase-locked detection techniques.

Two-Photon-Induced Photoluminescence Circular Dichroism. TPPL-CD measurements of the samples were carried out with 100 fs laser pulses (Chameleon Vision S) at a wavelength of 800−1000 nm. The initial input beam polarization was set by means of a Glan-Taylor polarizer, followed by PEM, which modulates between left and right circular polarized pulses at 50 kHz. The CP pulses were incident normally on the chiral films, and the generated photoluminescent photons were then collected onto a PMT in transmission mode after dual filtering using copper sulfate solution and a band-pass filter (BG40, Thorlabs). The PMT signal was converted to a voltage signal using a trans-impedance amplifier. The TPPL-CD signal was then measured using standard phase-locked detection techniques through a lock-in amplifier (Signal Recovery 7270).

Spectral Measurement of Two-Photon-Induced Photoluminescence. The spectral measurements of the TPPL signal were performed in the same setup as the TPPL-CD. The only difference was that the generated photoluminescent photons after filtering out the fundamental beam was focused to a fiber-based Ocean Optics spectrometer (USB 4000). The data were acquired for 60 s for better signal-to-noise ratio.

AUTHOR INFORMATION

Corresponding Author

*E-mail: ambarish@ece.iisc.ernet.in.

Author Contributions

#H. J. Singh and Saumitra are equal contributors, listed alphabetically.

Notes

The authors declare no competing financial interest.

ACKNOWLEDGMENTS

Helpful discussions with Pushpendu Das, the usage of the facilities in the Micro and Nano Characterization Facility (MNCF, CeNSE) at IISc, and funding from the Department of Biotechnology, as well as the Science and Engineering Research Board, are gratefully acknowledged. This work is partially supported by the Ministry of Communication and Information Technology under a grant for the Centre of Excellence in Nanoelectronics, Phase II. B.J. acknowledges support from the Department of Science and Technology and the Department of Biotechnology, Government of India.

REFERENCES

(1) Maier, S. A. *Plasmonics: Fundamentals and Applications*; Springer Science & Business Media, 2007.

(2) Willets, K. A.; Van Duyne, R. P. Localized surface plasmon resonance spectroscopy and sensing. *Annu. Rev. Phys. Chem.* **2007**, *58*, 267−297.

(3) Anker, J. N.; Hall, W. P.; Lyandres, O.; Shah, N. C.; Zhao, J.; Van Duyne, R. P. Biosensing with plasmonic nanosensors. *Nat. Mater.* **2008**, *7*, 442−453.

(4) Atwater, H. A.; Polman, A. Plasmonics for improved photovoltaic devices. *Nat. Mater.* **2010**, *9*, 205−213.

(5) Linic, S.; Christopher, P.; Ingram, D. B. Plasmonic-metal nanostructures for efficient conversion of solar to chemical energy. *Nat. Mater.* **2011**, *10*, 911−921.

(6) Kawata, S.; Inouye, Y.; Verma, P. Plasmonics for near-field nano-imaging and superlensing. *Nat. Photonics* **2009**, *3*, 388−394.

(7) Jain, P. K.; El-Sayed, I. H.; El-Sayed, M. A. Au nanoparticles target cancer. *Nano Today* **2007**, *2*, 18−29.

(8) West, J. L.; Halas, N. J. Engineered nanomaterials for biophotonics applications: improving sensing, imaging, and therapeutics. *Annu. Rev. Biomed. Eng.* **2003**, *5*, 285−292.

(9) Kneipp, K.; Wang, Y.; Kneipp, H.; Perelman, L. T.; Itzkan, I.; Dasari, R. R.; Feld, M. S. Single molecule detection using surface-enhanced Raman scattering (SERS). *Phys. Rev. Lett.* **1997**, *78*, 1667.

(10) Stiles, P. L.; Dieringer, J. A.; Shah, N. C.; Van Duyne, R. P. Surface-enhanced Raman spectroscopy. Annu. *Annu. Rev. Anal. Chem.* **2008**, *1*, 601−626.

(11) Campion, A.; Kambhampati, P. Surface-enhanced Raman scattering. *Chem. Soc. Rev.* **1998**, *27*, 241−250.

(12) Dostálek, J.; Knoll, W. Biosensors based on surface plasmon-enhanced fluorescence spectroscopy (Review). *Biointerphases* **2008**, *3*, FD12−FD22.

(13) Aslan, K.; Gryczynski, I.; Malicka, J.; Matveeva, E.; Lakowicz, J. R.; Geddes, C. D. Metal-enhanced fluorescence: an emerging tool in biotechnology. *Curr. Opin. Biotechnol.* **2005**, *16*, 55−62.

(14) Hou, W.; Cronin, S. B. A Review of Surface Plasmon Resonance-Enhanced Photocatalysis. *Adv. Funct. Mater.* **2013**, *23*, 1612−1619.

(15) Paria, D.; Roy, K.; Singh, H. J.; Kumar, S.; Raghavan, S.; Ghosh, A.; Ghosh, A. Ultrahigh Field Enhancement and Photoresponse in Atomically Separated Arrays of Plasmonic Dimers. *Adv. Mater.* **2015**, *27*, 1751−1758.

(16) Wei, Q.-H.; Su, K.-H.; Durant, S.; Zhang, X. Plasmon resonance of finite one-dimensional Au nanoparticle chains. *Nano Lett.* **2004**, *4*, 1067−1071.

(17) Krenn, J.; Salerno, M.; Felidj, N.; Lamprecht, B.; Schider, G.; Leitner, A.; Aussenegg, F.; Weeber, J.; Dereux, A.; Goudonnet, J. Light field propagation by metal micro-and nanostructures. *J. Microsc.* **2001**, *202*, 122−128.

(18) Haynes, C. L.; McFarland, A. D.; Zhao, L.; Van Duyne, R. P.; Schatz, G. C.; Gunnarsson, L.; Prikulis, J.; Kasemo, B.; Käll, M. Nanoparticle optics: the importance of radiative dipole coupling in two-dimensional nanoparticle arrays. *J. Phys. Chem. B* **2003**, *107*, 7337−7342.

(19) Johnson Singh, H.; Ghosh, A. Porous Three Dimensional Arrays of Plasmonic Nanoparticles. *J. Phys. Chem. C* **2012**, *116*, 19467−19471.

(20) Pendry, J. A chiral route to negative refraction. *Science* **2004**, *306*, 1353−1355.

(21) Gansel, J. K.; Thiel, M.; Rill, M. S.; Decker, M.; Bade, K.; Saile, V.; von Freymann, G.; Linden, S.; Wegener, M. Gold helix photonic metamaterial as broadband circular polarizer. *Science* **2009**, *325*, 1513−1515.

(22) Hendry, E.; Carpy, T.; Johnston, J.; Popland, M.; Mikhaylovskiy, R.; Lapthorn, A.; Kelly, S.; Barron, L.; Gadegaard, N.; Kadodwala, M. *Nat. Nanotechnol.* **2010**, *5*, 783−787.

(23) Boyd, R. W. *Nonlinear Optics*; Academic Press, 2003.

(24) Kauranen, M.; Zayats, A. V. Nonlinear plasmonics. *Nat. Photonics* **2012**, *6*, 737−748.

(25) Stockman, M. I.; Bergman, D. J.; Anceau, C.; Brasselet, S.; Zyss, J. Enhanced second-harmonic generation by metal surfaces with nanoscale roughness: nanoscale dephasing, depolarization, and correlations. *Phys. Rev. Lett.* **2004**, *92*, 057402.

(26) Wagnière, G. H. *Linear and Nonlinear Optical Properties of Molecules*; Weinheim: New York, 1993.

(27) Mooradian, A. Photoluminescence of metals. *Phys. Rev. Lett.* **1969**, *22*, 185.

(28) Boyd, G.; Yu, Z.; Shen, Y. Photoinduced luminescence from the noble metals and its enhancement on roughened surfaces. *Phys. Rev. B: Condens. Matter Mater. Phys.* **1986**, *33*, 7923.

(29) Wilcoxon, J.; Martin, J.; Parsapour, F.; Wiedenman, B.; Kelley, D. Photoluminescence from nanosize gold clusters. *J. Chem. Phys.* **1998**, *108*, 9137−9143.

(30) Biagioni, P.; Celebrano, M.; Savoini, M.; Grancini, G.; Brida, D.; Mátéfi-Tempfli, S.; Mátéfi-Tempfli, M.; Duò, L.; Hecht, B.; Cerullo, G. Dependence of the two-photon photoluminescence yield of gold

DOI: 10.1021/acsphotonics.6b00087
ACS Photonics 2016, 3, 863−868

nanostructures on the laser pulse duration. *Phys. Rev. B: Condens. Matter Mater. Phys.* **2009**, *80*, 045411.
(31) Loumaigne, M.; Richard, A.; Laverdant, J.; Nutarelli, D.; Débarre, A. Ligand-induced anisotropy of the two-photon luminescence of spherical gold particles in solution unraveled at the single particle level. *Nano Lett.* **2010**, *10*, 2817−2824.
(32) Wang, D.-S.; Hsu, F.-Y.; Lin, C.-W. Surface plasmon effects on two photon luminescence of gold nanorods. *Opt. Express* **2009**, *17*, 11350−11359.
(33) Imura, K.; Nagahara, T.; Okamoto, H. Plasmon mode imaging of single gold nanorods. *J. Am. Chem. Soc.* **2004**, *126*, 12730−12731.
(34) Imura, K.; Nagahara, T.; Okamoto, H. Near-field two-photon-induced photoluminescence from single gold nanorods and imaging of plasmon modes. *J. Phys. Chem. B* **2005**, *109*, 13214−13220.
(35) Castro-Lopez, M.; Brinks, D.; Sapienza, R.; van Hulst, N. F. Aluminum for nonlinear plasmonics: resonance-driven polarized luminescence of Al, Ag, and Au nanoantennas. *Nano Lett.* **2011**, *11*, 4674−4678.
(36) Wang, H.; Huff, T. B.; Zweifel, D. A.; He, W.; Low, P. S.; Wei, A.; Cheng, J.-X. In vitro and in vivo two-photon luminescence imaging of single gold nanorods. *Proc. Natl. Acad. Sci. U. S. A.* **2005**, *102*, 15752−15756.
(37) Park, J.; Estrada, A.; Sharp, K.; Sang, K.; Schwartz, J. A.; Smith, D. K.; Coleman, C.; Payne, J. D.; Korgel, B. A.; Dunn, A. K. Two-photon-induced photoluminescence imaging of tumors using near-infrared excited gold nanoshells. *Opt. Express* **2008**, *16*, 1590−1599.
(38) Wang, Q.-Q.; Han, J.-B.; Guo, D.-L.; Xiao, S.; Han, Y.-B.; Gong, H.-M.; Zou, X.-W. Highly efficient avalanche multiphoton luminescence from coupled Au nanowires in the visible region. *Nano Lett.* **2007**, *7*, 723−728.
(39) Kim, H.; Xiang, C.; Guell, A. G.; Penner, R. M.; Potma, E. O. Tunable two-photon excited luminescence in single gold nanowires fabricated by lithographically patterned nanowire electrodeposition. *J. Phys. Chem. C* **2008**, *112*, 12721−12727.
(40) Schuck, P.; Fromm, D.; Sundaramurthy, A.; Kino, G.; Moerner, W. Improving the mismatch between light and nanoscale objects with gold bowtie nanoantennas. *Phys. Rev. Lett.* **2005**, *94*, 017402.
(41) Durr, N. J.; Larson, T.; Smith, D. K.; Korgel, B. A.; Sokolov, K.; Ben-Yakar, A. Two-photon luminescence imaging of cancer cells using molecularly targeted gold nanorods. *Nano Lett.* **2007**, *7*, 941−945.
(42) Wu, X.; Ming, T.; Wang, X.; Wang, P.; Wang, J.; Chen, J. High-photoluminescence-yield gold nanocubes: for cell imaging and photothermal therapy. *ACS Nano* **2009**, *4*, 113−120.
(43) Belardini, A.; Larciprete, M.; Centini, M.; Fazio, E.; Sibilia, C.; Chiappe, D.; Martella, C.; Toma, A.; Giordano, M.; de Mongeot, F. B. Circular dichroism in the optical second-harmonic emission of curved gold metal nanowires. *Phys. Rev. Lett.* **2011**, *107*, 257401.
(44) Huttunen, M. J.; Bautista, G.; Decker, M.; Linden, S.; Wegener, M.; Kauranen, M. Nonlinear chiral imaging of subwavelength-sized twisted-cross gold nanodimers [Invited]. *Opt. Mater. Express* **2011**, *1*, 46−56.
(45) Valev, V.; Smisdom, N.; Silhanek, A.; De Clercq, B.; Gillijns, W.; Ameloot, M.; Moshchalkov, V.; Verbiest, T. Plasmonic ratchet wheels: switching circular dichroism by arranging chiral nanostructures. *Nano Lett.* **2009**, *9*, 3945−3948.
(46) Fan, Z.; Govorov, A. O. Plasmonic circular dichroism of chiral metal nanoparticle assemblies. *Nano Lett.* **2010**, *10*, 2580−2587.
(47) Singh, J. H.; Nair, G.; Ghosh, A.; Ghosh, A. Wafer scale fabrication of porous three-dimensional plasmonic metamaterials for the visible region: chiral and beyond. *Nanoscale* **2013**, *5*, 7224−7228.
(48) Hrudey, P. C.; Westra, K. L.; Brett, M. J. Highly Ordered Organic Alq3 Chiral Luminescent Thin Films Fabricated by Glancing-Angle Deposition. *Adv. Mater.* **2006**, *18*, 224−228.
(49) Hawkeye, M. M.; Brett, M. J. Glancing angle deposition: Fabrication, properties, and applications of micro-and nanostructured thin films. *J. Vac. Sci. Technol., A* **2007**, *25*, 1317−1335.
(50) Nair, G.; Singh, H. J.; Paria, D.; Venkatapathi, M.; Ghosh, A. Plasmonic interactions at close proximity in chiral geometries: route toward broadband chiroptical response and giant enantiomeric sensitivity. *J. Phys. Chem. C* **2014**, *118*, 4991−4997.
(51) Nair, G.; Singh, J. H.; Ghosh, A. Tuning the chiro-plasmonic response using high refractive index-dielectric templates. *J. Mater. Chem. C* **2015**, *3*, 6831.
(52) Auguié, B.; Alonso-Gómez, J. L.; Guerrero-Martínez, A.; Liz-Marzán, L. M. Fingers crossed: Optical activity of a chiral dimer of plasmonic nanorods. *J. Phys. Chem. Lett.* **2011**, *2*, 846−851.
(53) Tinoco, I., Jr Two-photon circular dichroism. *J. Chem. Phys.* **1975**, *62*, 1006−1009.
(54) Power, E. Two-photon circular dichroism. *J. Chem. Phys.* **1975**, *63*, 1348−1350.
(55) Shahbazyan, T. V. Theory of plasmon-enhanced metal photoluminescence. *Nano Lett.* **2012**, *13*, 194−198.
(56) Kuzyk, A.; Schreiber, R.; Fan, Z.; Pardatscher, G.; Roller, E.-M.; Högele, A.; Simmel, F. C.; Govorov, A. O.; Liedl, T. DNA-based self-assembly of chiral plasmonic nanostructures with tailored optical response. *Nature* **2012**, *483*, 311−314.
(57) Savoini, M.; Wu, X.; Celebrano, M.; Ziegler, J.; Biagioni, P.; Meskers, S. C.; Duò, L.; Hecht, B.; Finazzi, M. Circular dichroism probed by two-photon fluorescence microscopy in enantiopure chiral polyfluorene thin films. *J. Am. Chem. Soc.* **2012**, *134*, 5832−5835.
(58) Toro, C.; Passier, R.; Diaz, C.; Tuuttila, T.; Rissanen, K.; Huuskonen, J.; Hernández, F. E. Unveiling Electronic Transitions in Three Novel Chiral Azo-Compounds Using Linear and Nonlinear Circular Dichroism: A Theoretical− Experimental Study. *J. Phys. Chem. A* **2011**, *115*, 1186−1193.
(59) Diaz, C.; Vesga, Y.; Echevarria, L.; Stará, I. G.; Starỳ, I.; Anger, E.; Shen, C.; Moussa, M. E. S.; Vanthuyne, N.; Crassous, J. Two-photon absorption and two-photon circular dichroism of hexahelicene derivatives: a study of the effect of the nature of intramolecular charge transfer. *RSC Adv.* **2015**, *5*, 17429−17437.
(60) Toro, C.; De Boni, L.; Lin, N.; Santoro, F.; Rizzo, A.; Hernandez, F. E. Two-Photon Absorption Circular Dichroism: A New Twist in Nonlinear Spectroscopy. *Chem. - Eur. J.* **2010**, *16*, 3504−3509.
(61) Gunde, K. E.; Richardson, F. Fluorescence-detected two-photon circular dichroism of Gd 3+ in trigonal Na 3 [Gd (C 4 H 4 O 5) 3]· 2NaClO 4· 6H 2 O. *Chem. Phys.* **1995**, *194*, 195−206.
(62) Ghosh, A.; Fischer, P. Controlled propulsion of artificial magnetic nanostructured propellers. *Nano Lett.* **2009**, *9*, 2243−2245.
(63) Fischer, P.; Ghosh, A. Magnetically actuated propulsion at low Reynolds numbers: towards nanoscale control. *Nanoscale* **2011**, *3*, 557−563.
(64) Ghosh, A.; Paria, D.; Singh, H. J.; Venugopalan, P. L.; Ghosh, A. Dynamical configurations and bistability of helical nanostructures under external torque. *Phys. Rev. E* **2012**, *86*, 031401.
(65) Venugopalan, P. L.; Sai, R.; Chandorkar, Y.; Basu, B.; Shivashankar, S.; Ghosh, A. Conformal cytocompatible ferrite coatings facilitate the realization of a nanovoyager in human blood. *Nano Lett.* **2014**, *14*, 1968−1975.

DOI: 10.1021/acsphotonics.6b00087
ACS Photonics 2016, 3, 863−868